Generic Sensor Modeling Using Pulse Method

By

Dennis L. Helder, Taeyoung Choi

Electrical Engineering Department

South Dakota State University

August, 2005

Generic Sensor Modeling Using Pulse Method

By

Dennis L. Helder, Taeyoung Choi

Electrical Engineering Department

South Dakota State University

August, 2005

Table of Contents

List of Tables

List of Figures

1 Introduction

Recent development of high spatial resolution satellites such as IKONOS, Quickbird and Orbview enable observation of the Earth's surface with sub-meter resolution. Compared to the 30 meter resolution of Landsat 5 TM, the amount of information in the output image was dramatically increased. In this era of high spatial resolution, the estimation of spatial quality of images is gaining attention. Historically, the Modulation Transfer Function (MTF) concept has been used to estimate an imaging system's spatial quality. Sometimes classified by target shapes, various methods were developed in laboratory environment utilizing sinusoidal inputs [1], periodic bar patterns and narrow slits [2]. On-orbit sensor MTF estimation was performed on 30-meter GSD Landsat 4 Thematic Mapper (TM) data from the bridge pulse target as a pulse input [3]. Because of a high resolution sensor's small Ground Sampling Distance (GSD), reasonably sized man-made edge, pulse, and impulse targets can be deployed on a uniform grassy area with accurate control of ground targets using tarps and convex mirrors [4]. All the previous work cited calculated MTF without testing the MTF estimator's

performance. In previous report, a numerical generic sensor model had been developed to simulate and improve the performance of on-orbit MTF estimating techniques. Results from the previous sensor modeling report that have been corporated into standard MTF estimation work include Fermi edge detection and the newly developed 4^{th} order modified Savitzky-Golay (MSG) interpolation technique. Noise sensitivity had been studied by performing simulations on known noise sources and a sensor model. Extensive investigation was done to characterize multi-resolution ground noise. Finally, angle simulation was tested by using synthetic pulse targets with angles from 2 to 15 degrees, several brightness levels, and different noise levels from both ground targets and imaging system.

As a continuing research activity using the developed sensor model, this report was dedicated to MTF estimation via pulse input method characterization using the Fermi edge detection and 4^{th} order MSG interpolation method. The relationship between pulse width and MTF value at Nyquist was studied including error detection and correction schemes. Pulse target angle sensitivity was studied by using synthetic targets angled from 2 to 12 degrees.

In this report, from the ground and system noise simulation, a minimum SNR value was suggested for a stable

MTF value at Nyquist for the pulse method. Target width error detection and adjustment technique based on a smooth transition of MTF profile is presented, which is specifically applicable only to the pulse method with 3 pixel wide targets.

2 Procedures

2.1 Generic Sensor Model

The output image from a sensor is not a faithful reproduction of the original ground truth. In other words, an imaging system degrades the spatial quality of its output image due to characteristics of the system optics, detectors, motion, and electronics blurring sources. Each intermediate blurring source is numerically described briefly in following sections.

2.1.1 Optical PSF

The Optical PSF refers to the impulse response of the sensor optics. A sharp bright point such as a star in space with a dark background, a convex mirror on the ground, or a fine pin-hole in the laboratory can approximate an impulse input to the sensor. Its spatial energy distribution over a small area on the focal plane through the telescope or optics is known as optical PSF. Usually, optical PSF is modeled by a 2-D Gaussian function,

$$PSF_{opt}(x,y) = \frac{1}{2\pi ab} e^{-x^2/2a^2} e^{-y^2/2b^2} \qquad (2.1)$$

The parameters 'a' and 'b' are standard deviations in the x and y directions, which determine the blurring extent due to the optics.

2.1.2 Detector PSF

The non-zero spatial area of each detector in the sensor array causes detector blurring. Incoming energy falling on a detector square is integrated over the spatial extent of the detector , i.e., each sensor is considered an integrating square or rectangle. The size of the detector rectangle is a variable for a sensor. Detector PSF can be modeled by using the rect function,

$$PSF_{det}(x,y) = rect(x/GIFOV)rect(y/GIFOV) \qquad (2.2)$$

where GIFOV is Ground-projected Instantaneous Field Of View, and the *rect* function is shown in Figure 2.1.

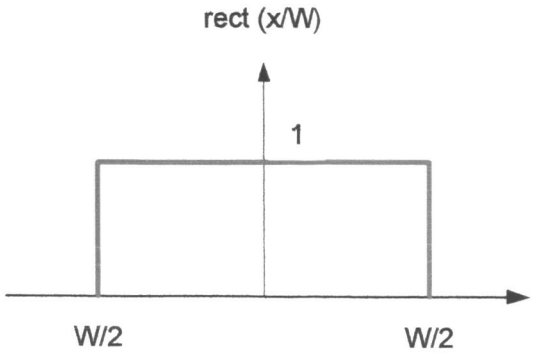

Figure 2.1. The 'rect' function plot.

2.1.3 Motion PSF

Because only a pushbroom scanner model will be considered, the focal plane moves in the along-track sensor direction while it images; this causes linear motion blurring. The sensor speed and line integration time are key factors of this model.

$$PSF_{Mot}(x,y) = rect(y/S) \tag{2.3}$$

$$\text{Where } S = sensor\ speed \times integration\ time. \tag{2.4}$$

2.1.4 Electronics PSF

Another source of blurring is due to sensor electronics. Usually, the signals from the detectors are lowpass filtered prior to sampling. This filtering process reduces high-frequency components from the signal to reduce aliasing effects. As a side effect of the anti-aliasing process, it causes spatial blurring in the imaging system. An example of the presample filter on the Multispectral Scanner (MSS) was shown as a three-pole Butterworth filter in [5]. Because there was no available information about typical pushbroom sensor electronics, this effect was

modeled by a simple first order 2-D Butterworth lowpass filter [5].

$$H(u,v) = \frac{1}{1+\left[D(u,v)/D_0\right]^2} \tag{2.5}$$

where $D(u,v)$ is defined as

$$D(u,v) = \left(u^2 + v^2\right)^{\frac{1}{2}}. \tag{2.6}$$

And u and v represent Fourier domain horizontal and vertical frequency variables.

This Butterworth lowpass transfer function does not cause a sharp discontinuity or ringing effect in spatial domain.

2.1.5 Atmospheric Effects and Noise Sources

A generic sensor model block diagram is shown in Figure 2.2. There is another source of blurring between the sensor model and ground target. However, atmospheric blurring is not considered in this generic sensor model because it is beyond the goal of this research and demands extensive development activity. A simplified assumption that atmospheric blurring is negligible compared to sensor blurring scales is invoked.

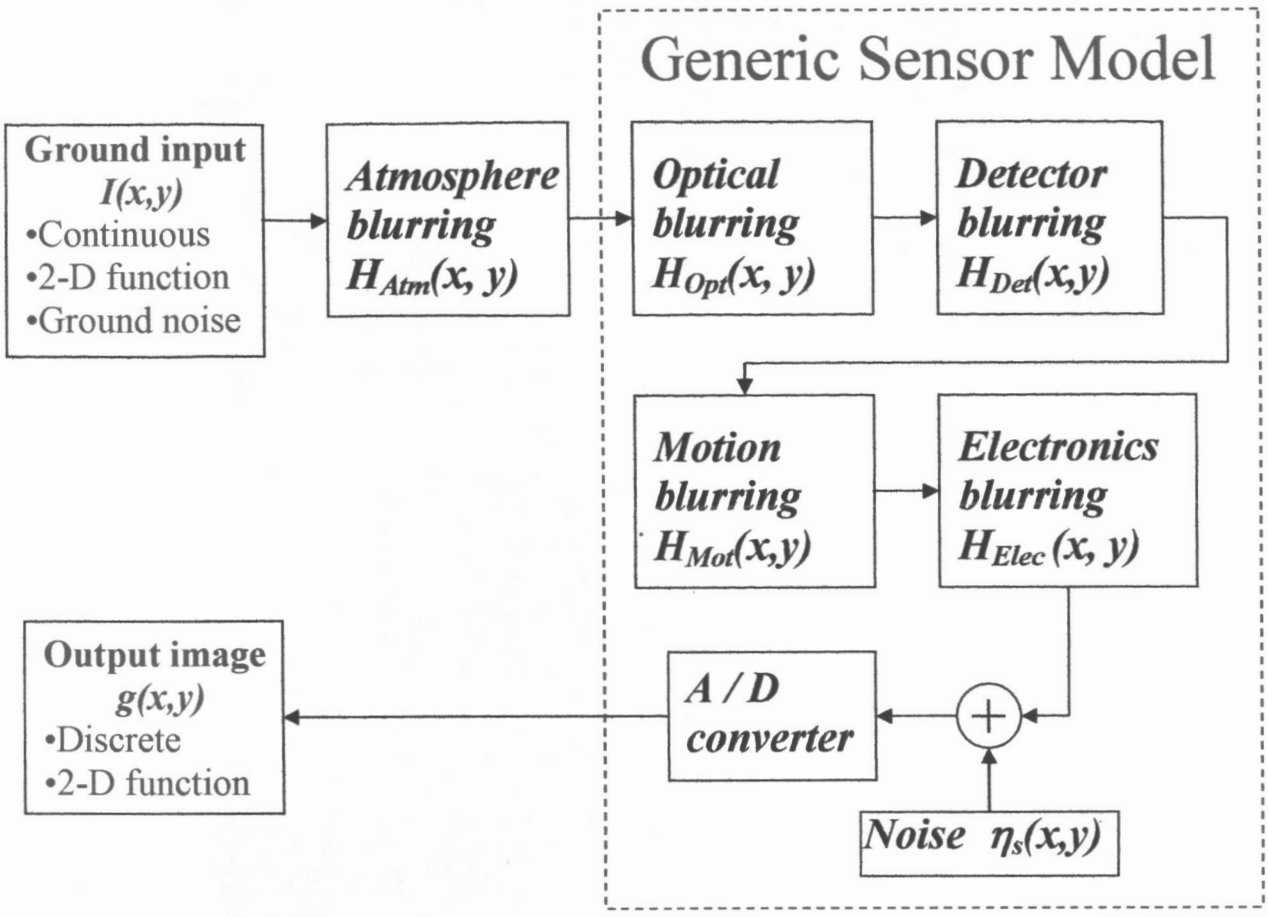

Figure 2.2. The generic sensor model block diagram.

There are two noise sources in Figure 2.2. One source is from the target, which is named as ground noise and another source is from the sensor itself defined as system noise. The former source is caused from the non-uniformity of the ground target that becomes the input to the sensor. Multi-resolution ground noise images were generated to form an artificial ground noise. The latter, system noise, is modeled as an image resolution scale simple white, Gaussian noise.

2.2 Synthetic Target Generation

Once a generic sensor model, and resulting PSF, is established, it is convolved with ideal synthetic pulse images. The edge angle was determined to be 6 degrees from true North, which was predetermined from typical field campaigns to cover at least two-pixels in the across-track direction. The edge angle was chosen by compromising between the length of target and desired pixel coverage across the edge direction. The original PSF and the synthetic images were finely sampled 20 times greater than the original GSD. Therefore, one pixel was interpolated by twenty sub-pixels. The synthetic pulse target is shown in Figure 2.3 along with convolution with the sensor model and subsequent resampling to the nominal GSD.

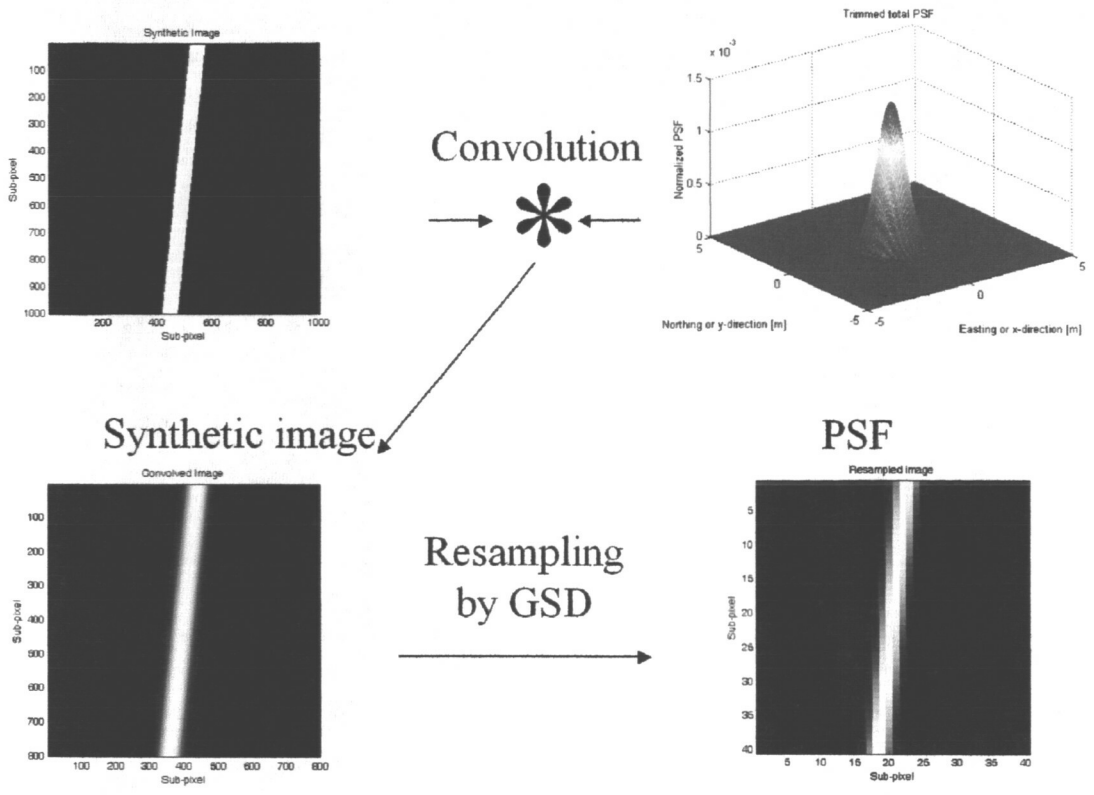

Figure 2.3. Synthetic pulse target generation procedures.

2.3 MTF Estimator

2.3.1 Basic Concept of Pulse method

A parametric Fermi function edge detection step was applied first to locate the exact edge location of the pulse target. Then the Pulse Response Function (PRF) was extracted by several interpolation techniques such as spline, sliding window or MSG filtering. Finally, the MTF is calculated by obtaining the Fourier transform ratio between the PRF and an ideal step pulse as shown in Figure 2.4.

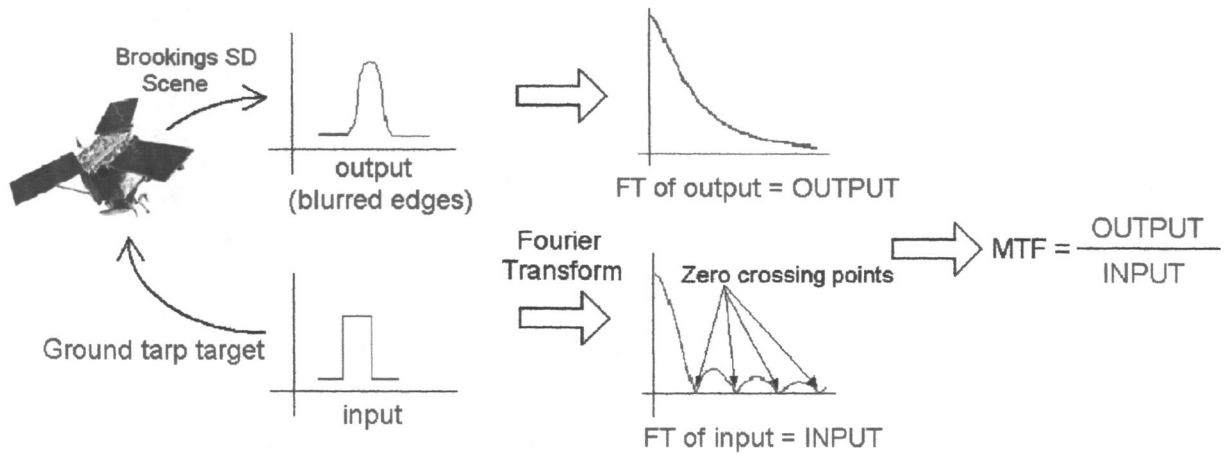

Figure 2.4. Pulse method.

2.3.2 Fermi Function Edge Detection

Instead of using a numerical edge detection method based on spline interpolation, an accurate model-based parametric method was applied to detect sub-pixel edge locations. The Fermi function was chosen [6] to fit to the ESF:

$$f(x) = \frac{a}{\exp\left[\frac{(x-b)}{c} - 1\right]} + d \qquad (2.7)$$

where a = amplitude of edge, b = edge location, c = curvature of edge, d = offset. Even though all the output parameters have important information (for example, the MTF

value is directly related to the 'c' value), only the 'b' value was needed from determination of the sub-pixel edge location. Figure 2.5 shows an output edge image with initial sub-pixel edge locations indicated by circles and final straight line using least square error fitting. Figure 2.6 shows a Fermi function, which is the best least-square fit to the seven closest data points to the initial edge location calculated from differentiation of the line. Following edge location for each row of pixels, a profile of the edge, or pulse, is obtained by aligning all edges to a common location in a single plot.

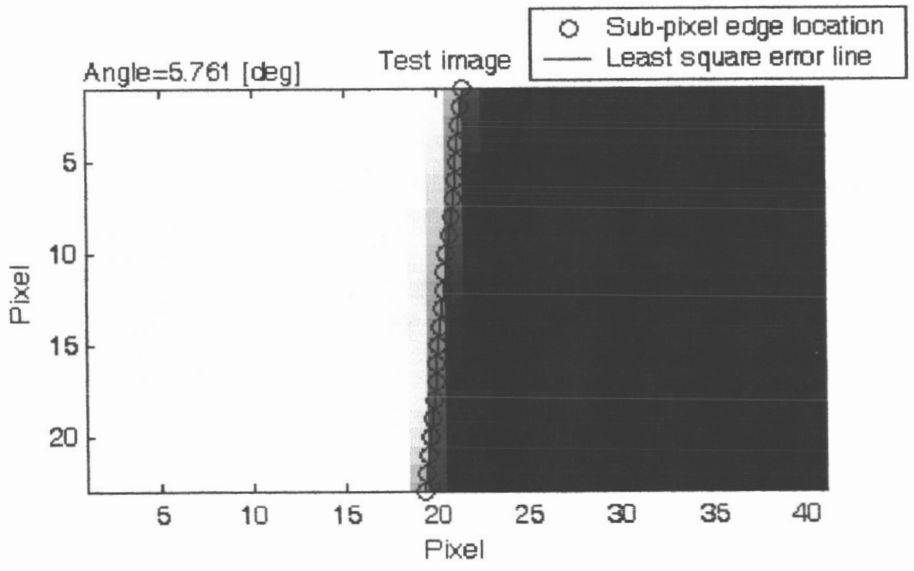

Figure 2.5. Cropped QuickBird satellite image of Stennistarp on September 7, 2002. Parametric sub-pixel edge locations are indicated as circles. A least square fitting line was calculated and drawn as a line through the circles.

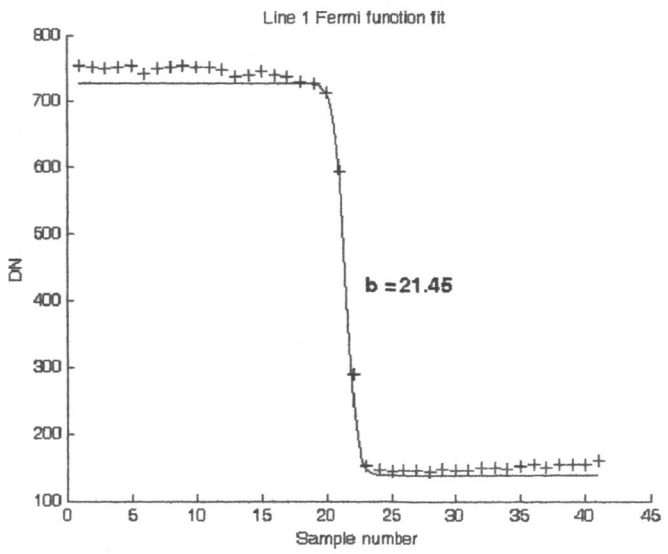

Figure 2.6. Seven closest points to the edge transition were used in Fermi function fit on line 1 in Figure 2.6.

2.3.3 Modified Savitzky-Golay (MSG) Interpolation Techniques

Spline, and sliding-window interpolation methods had been applied on 2000 to 2002 target images for edge, pulse and distance techniques. Recently MSG filtering algorithms have been developed for more accurate estimation of the original MTF. The final goal of the interpolation methods is to get a uniformly sub-sampled (20 times finer sampled) edge or pulse profile from randomly oversampled input data points.

Assume a digital filter applied to a series of equally spaced data values $f_i \equiv f(t_i)$, where $t_i = t_0 + i\Delta$ for some constant sample spacing Δ and $i = \ldots -2,-1,0,1,2\ldots$. A digital filter can be defined as [7].

$$g_i = \sum_{n=-n_L}^{n_R} c_n f_{i+n} \tag{2.8}$$

This is the basic form of a finite impulse response (FIR) filter shape. The output of the filter, g_i, is determined by the filter coefficients, c_n, with the linear combination of f_i. The summation indicator n_L is the number of points used 'to the left' of data point i, while n_R is the number of points used 'to the right.' For better understanding of Savitzky-Golay filtering for some fixed $n_R = n_L$, the output of the filter will be a moving window averaging filter with the constants $c_n = \frac{1}{(n_L + n_R + 1)}$. Assume the underlying function describing the data is a higher order function. The idea of Savitzky-Golay filtering is to find filter coefficients c_n that preserve higher moments; to approximate the underlying function within the moving window not by a constant whose estimate is the average of the data in the window, but by a polynomial of higher order, typically quadratic. A least-squares fit polynomial to all the $n_L + n_R + 1$ points in the moving window was found for each point f_i, and then set g_i to be the value of that polynomial at point i. When the window is shifted to the next point f_{i+1}, a whole new least-square process is done for the new window. Since least-

square fitting can be found by linear matrix inversion, the fitted polynomial coefficients are linear to the data points. Unfortunately, this linear combination is a basic assumption only for some constant sample spacing input as we mention at the start of this section.

A major problem started with accumulated data points as shown in Figure 2.7 after edge location alignment. All the input data point locations were randomly distributed rather than uniformly spaced. As a result, we could not apply a linear operation with a non-linear input. Instead of finding the coefficient matrix, we found the best fitting second order polynomial to the data points using the Matlab 'fmeansearch.m' function [8] within the moving window which is shown in Figure 2.7(a) as the black line in the blue window area. Then the middle point of this window was evaluated by the n-th order polynomial. Because the shifting step of the window was fixed to 0.05 pixels, the output of this 4th order polynomial is illustrated in Figure 2.7(b). Finally, all the evaluation points calculated by the fitted fourth order polynomial from each shifted window were used to construct an edge (or pulse) average profile.

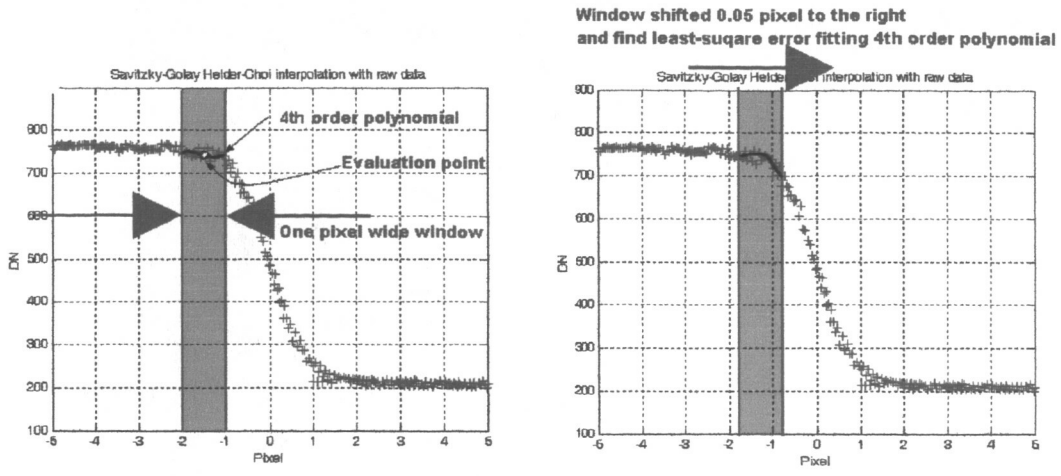

(a) 4^{th} order fitting line (b) Window shifting

Figure 2.7. Modified Savitzky-Golay filtering with 1-pixel window and 4th order polynomial fitting.

3 Result and Analysis

3.1 Generic Sensor Model Generation

Based on Section 2.1, there were six parameters to be chosen in our model. Those were parameters for optical, detector, motion, and electronic blurring. Because Quickbird and IKONOS were private satellites, no detailed sensor information was available. However, the overall LSF of the sensor in the panchromatic band had been measured in earlier analyses at the SDSU Image Processing Laboratory. Consequently, the following modeling parameters are not exact quantities for the sensor, but derived and chosen for PSF generation such that an overall FWHM of the LSF would be 1.12 meters.

3.1.1 Optical PSF

The first two parameters represented in-track and cross-track direction Gaussian blurring as explained in the equation 2.1. A symmetric value 0.39 has been chosen for 'a' and 'b' to make the FWHM of the optical PSF about 0.9 meter.

3.1.2 Detector PSF

Incoming energy excited on one detector was averaged by the non-zero size of detector area. The response was characterized by the rectangle function. We assumed that detectors were 1-meter squares as propagated from the sensor to the ground.

3.1.3 Motion PSF

Satellite motion blurring is one-dimensional blurring along the motion direction. The parameter 's' is a combination of satellite speed and integration time. Because there is no information of integration time, we assumed 's' to be 0.25 meter with amplitude 0.06.

3.1.4 Electronics PSF

A first order 2D Butterworth filter with 1.4 cycles per pixel cut-off frequency was employed as the electronic PSF. The FWHM of the PSF was less than 0.25 meters which

contributed a small amount of blurring to the net PSF. This electronic PSF was symmetric in both the spatial and frequency domains.

3.1.5 Net PSF

The net or total sensor PSF was calculated by convolving the optical PSF, detector PSF, motion PSF, and electronics PSF as expressed in equation 3.1.

$$PSF_{net}(x,y) = PSF_{opt}(x,y) * PSF_{\det}(x,y) * PSF_{mot}(x,y) * PSF_{elec}(x,y). \qquad (3.1)$$

After convolution, the zero background area was trimmed to a 5-meter square for calculation convenience. The net PSF is shown in Figure 3.1.

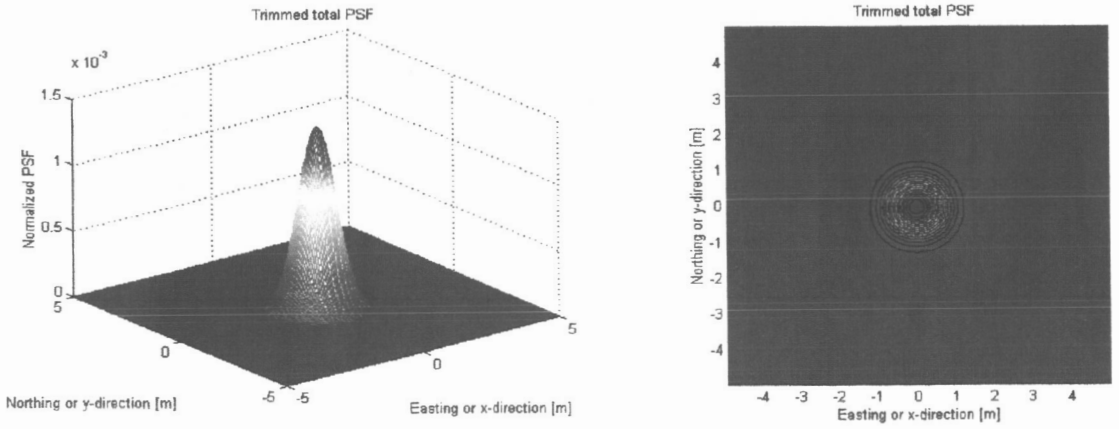

Figure 3.1. The net PSF

The PSF was normalized by the area under the curve to maintain the original average image value after convolution.

The net PSF was not symmetric because the along-track directional motion blurring was included. As shown in Figure 3.2, the difference between the two orthogonal FWHM values was 0.0141 meters. This effect is more apparent in the corresponding LSF and MTF overplots in Figure 3.3. The narrower cross track direction LSF resulted in a larger MTF value at each frequency point in Figure 3.3 except at DC. This net PSF was applied to all the synthetic edge and pulse targets as a generic sensor model to produce synthetic output images. Thus, the exact MTF information was known before MTF estimators were applied to the output image. All the results from the MTF estimators were compared to the original MTF from the model.

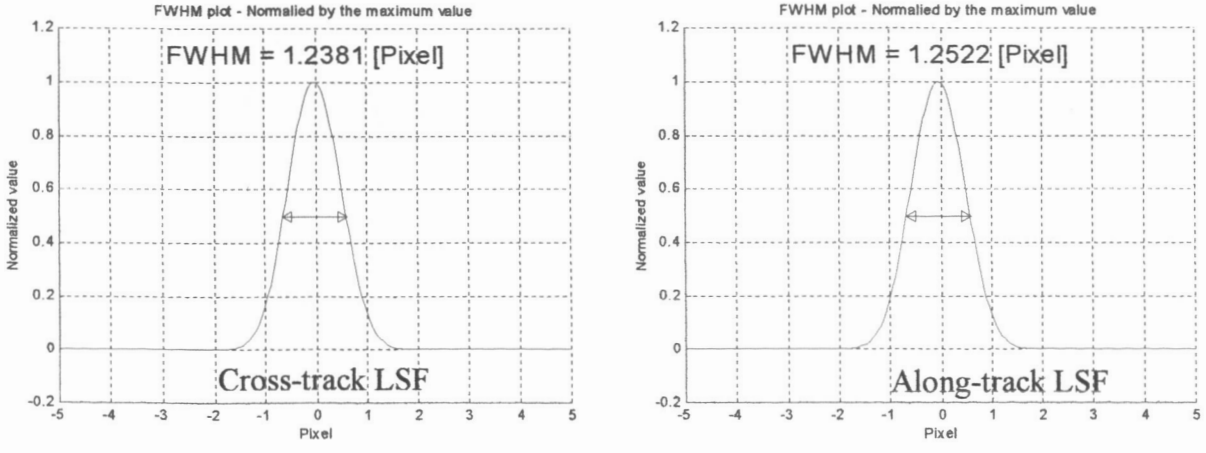

Figure 3.2. The net LSF in along and cross track direction.

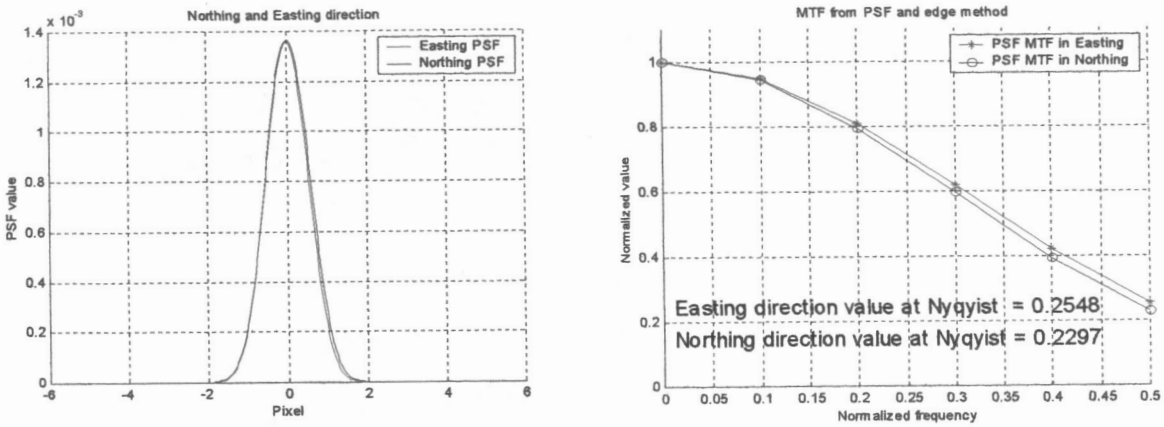

Figure 3.3. LSF and MTF over plots in along and cross track direction.

3.2 Noise Free Synthetic Pulse Target Generation

Once a sensor model was established, synthetic pulse targets were prepared to be processed as inputs to the synthetic imaging system. From linear systems theory, the operation transferring the input to the output is described as a convolution process. The synthetic input target was designed to have the same sub-pixel resolution as the system PSF. After two dimensional convolution between a PSF and a synthetic target, the convolved image was resampled to the desired GSD. Because this sensor model was designed to be close to the IKONOS panchromatic band, a one-meter grid was chosen to be the output GSD.

The process flow diagram is shown in Figure 3.4. The pulse width was predetermined to be three times the GSD in order to locate the Nyquist frequency on the maximum of the first side lobe when the input pulse is Fourier transformed. The DN value of the pulse was 1200 DN against a 100 DN background as shown in Figure 3.5.

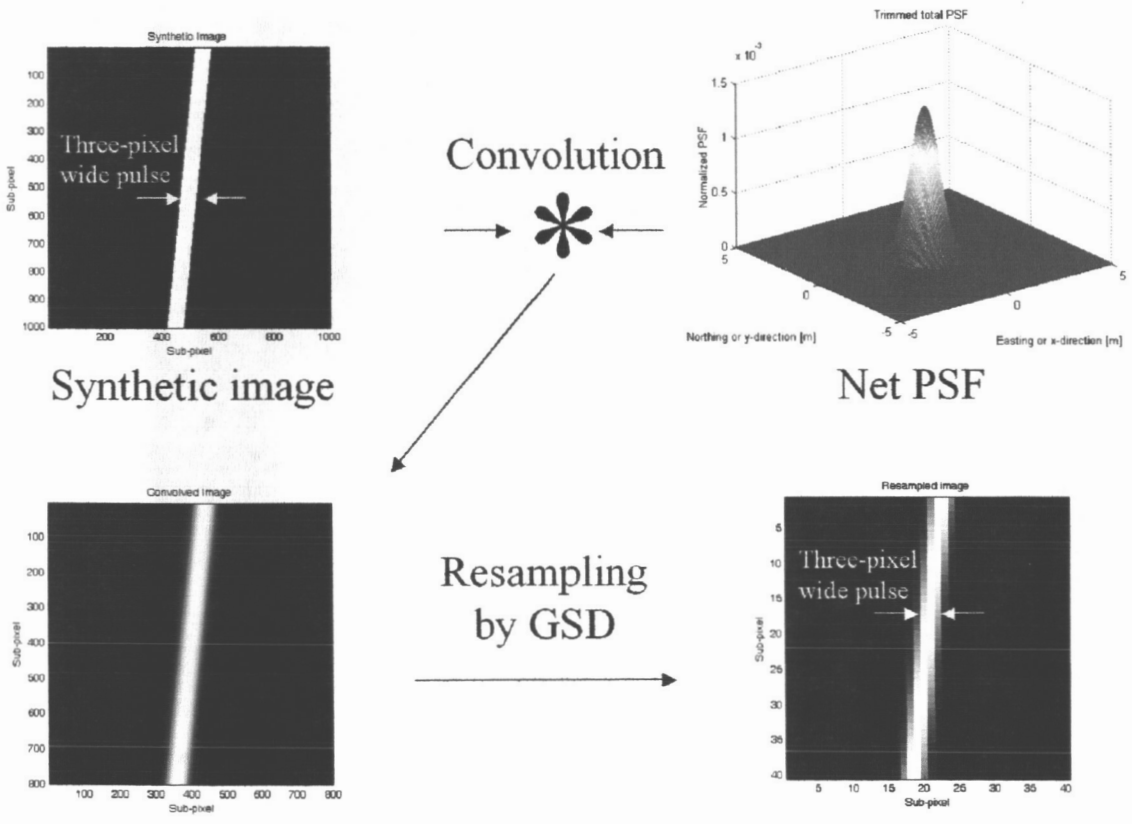

Figure 3.4. Noiseless synthetic pulse generation process.

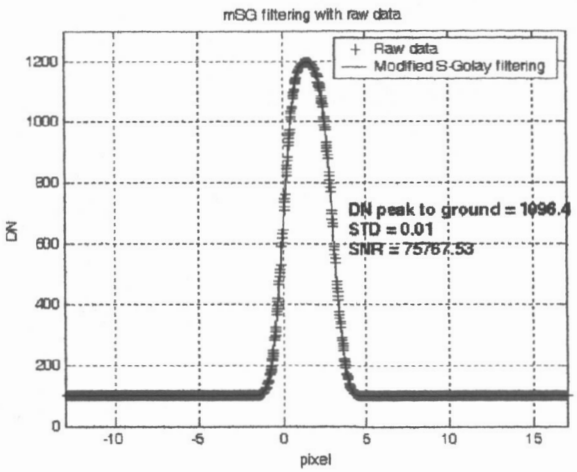

Figure 3.5. PRF of synthetic pulse using MSG filtering.

3.3 Pulse MTF Estimator Performance

A six-degree synthetic pulse target was generated and processed by using Fermi function edge detection and MSG interpolation. As shown in Figure 3.6, a Pulse Response Function (PRF) was calculated instead of a LSF due to the nature of the pulse method. Absolute PRF difference between the original and estimated LSF was 0.07% in spatial domain, which resulted in as 4.1% under-estimation from the original MTF value. Corresponding results plots are shown in Figure 3.6 and Table 3.1. This simulation was performed in a noise-free situation.

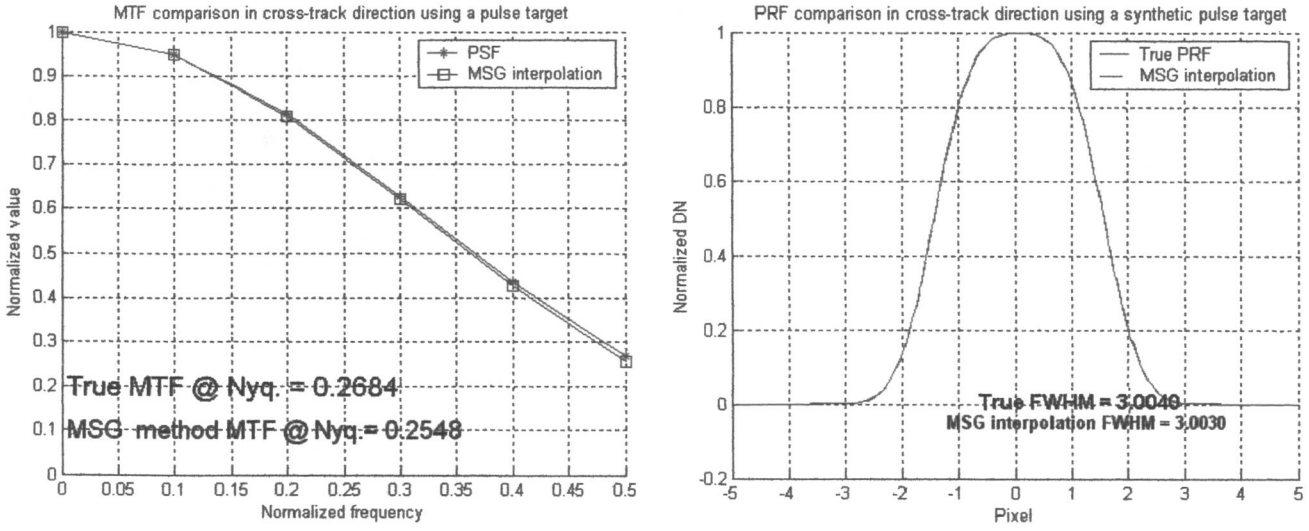

Figure 3.6. MTF estimator simulation over plots using pulse method.

Table 3.1. MTF estimator simulation results using pulse method.

Values	Original	MSG
FWHM of PRF [m]	3.0040	3.0020 (-0.07%)
MTF at Nyquist [cycle/pixel]	0.2684	0.2575 (-4.1%)

3.4 Noise Simulation

In the generic sensor model block diagram from Figure 2.2, there were two major noise sources: ground based and system based. Ground noise is caused by actual non-uniformity of the target, which was added before the sensor block. It was defined as a sum of multiple spatial resolutions from 5 cm to 1 meter with 5 cm steps. The system noise was added after sampling to the desired GSD.

3.4.1 Signal-to-Noise Ratio (SNR) Definition

The meaning of signal and noise should be defined with reference to in a pulse target profile. For a pulse target, the difference between the maximum value in the PRF and the average grass area DN level were divided by the one-sigma standard deviation noise estimate of the background areas as shown in Figure 3.7.

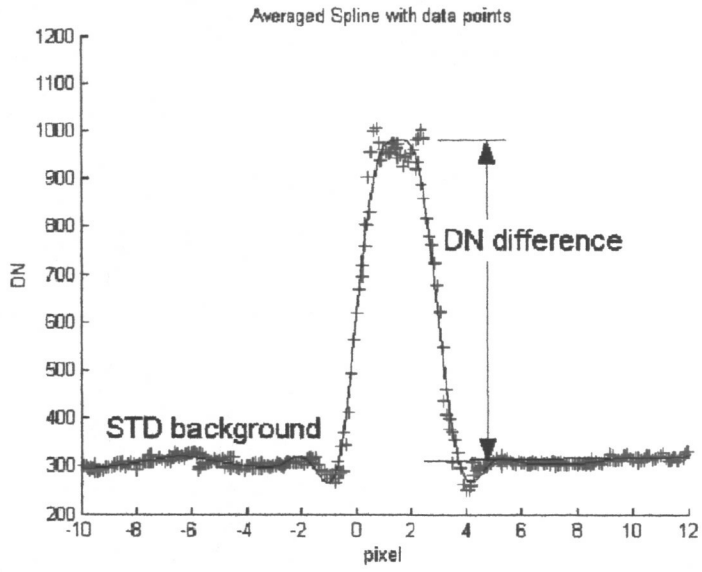

Figure 3.7. Signal-to-Noise ratio for pulse target.

3.4.2 System Noise Simulation

System noise simulation was performed without incorporating ground noise. The system noise was modeled as a white Gaussian noise process, which is a widely accepted characteristic of thermal noise. As shown in the block diagram in Section 2.1.5, noise was added after the sampling process, but before the scene was processed by the MTF estimator. To avoid a large number of calculations introduced by convolution, only one 6-degree edge target with edge transition from 200 to 1200 DN was used with a fixed DN difference in uniform areas. Ninety-nine different noise levels were tested from σ=2DN to σ=100DNwith a step

size of 1 DN. The MTF at Nyquist was estimated from each noisy image and plotted on Figure 3.8 as a function of SNR.

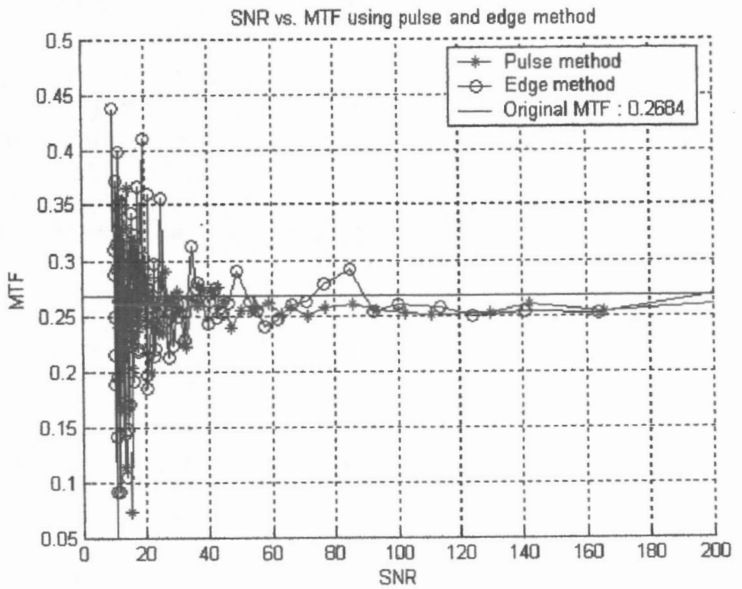

Figure 3.8. SNR vs. MTF value at Nyquist plot from system noise pulse and edge target simulation.

In Figure 3.8, the solid red line is the true value of the MTF at Nyquist. The results shown in Figure 3.8 suggest that a reliable MTF at Nyquist estimate can be obtained with a lower SNR using a pulse target as apposed to an edge target. For an edge target, an SNR $\geq$ 100 is suggested for reliable estimations. For the pulse target an SNR $\geq$ 50 is adequate. In both cases the estimated error tends to increase exponentially at lower SNR. Lastly, in both cases, the estimates tend to underestimate the MTF even at very high SNR's.

3.4.3 Ground Noise Simulation

The purpose of this simulation was to model the effects of ground noise to understand what SNR is needed with ground targets in order to achieve an accurate MTF estimate. This is particularly important for the pulse target approach since the background level is determined by the actual grassy surface and is not controlled by artificial target materials. As explained for the system noise case, ground noise simulation was performed in the absence of system noise. Firstly, the ground noise model was designed and characterized, and then it was added to a synthetic pulse target before convolution with a sensor model. Secondly, the output image was resampled to a desired GSD and it was processed by the pulse method MTF estimator.

3.4.3.1 Ground Noise Modeling

Non-uniformity on the ground was modeled as a sum of multiple sub-pixel wide sense stationary (WSS) white Gaussian noise images. The variance of each sub-resolution noise image was fixed to be 100. In Figure 3.9, noise images are shown in sub-pixel resolution from 1 sub-pixel

to 20 sub-pixel size squares. For each resolution level, the grid origin was randomly chosen within the GSD area in the 'x' and 'y' direction to achieve random phasing of sub-pixel grids. But these random origin locations were bounded by the minimum resolution, which was on a 5 cm grid in both 'x' and 'y' directions. Addition of twenty Gaussian random fields yields a Gaussian random field. The overall noise variance is then given by a linear sum of the individual variances. This result is consistent with the Central Limit Theorem. As a result of the addition process, the variance of the ground noise model was 2000.

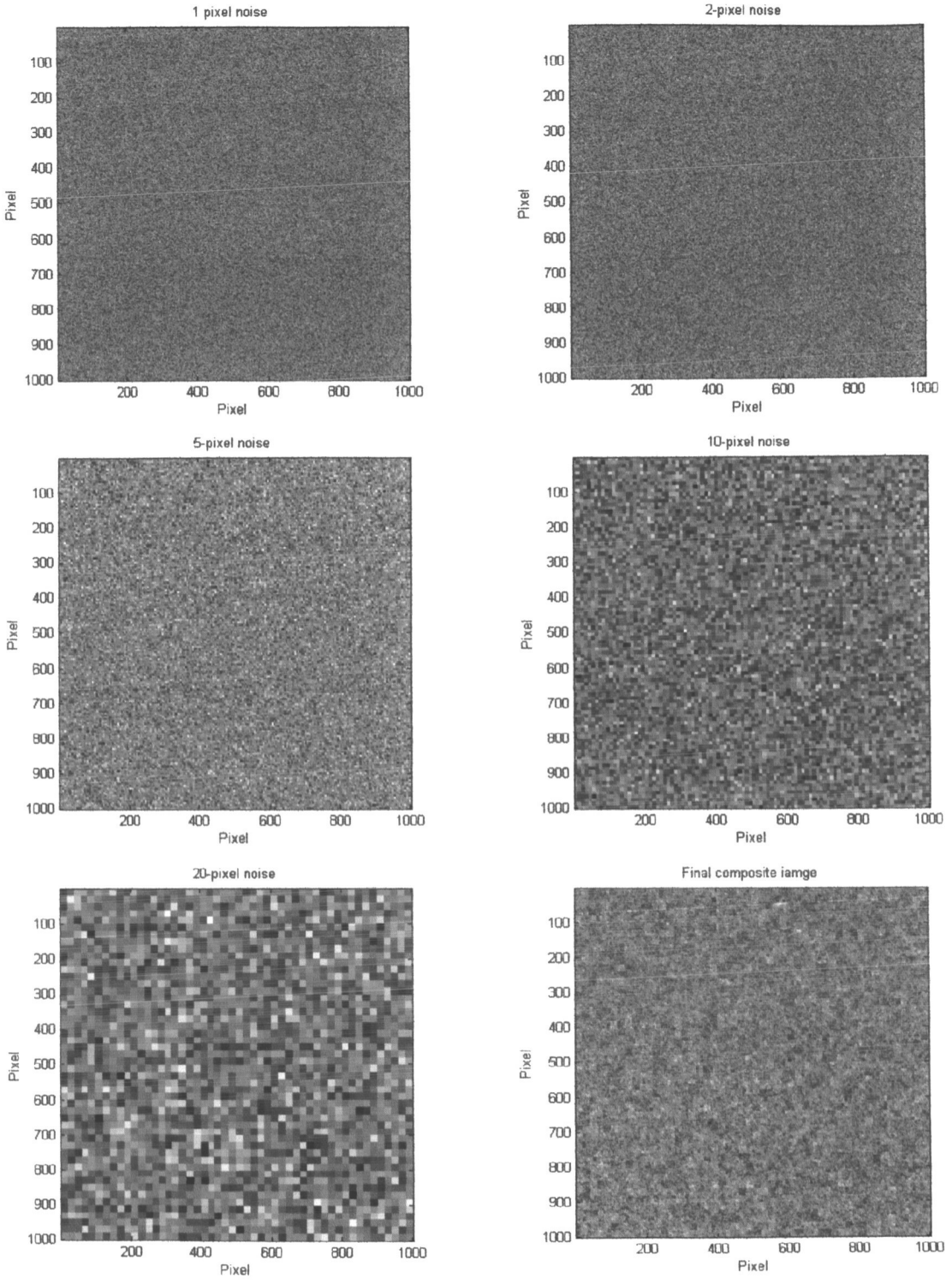

Figure 3.9. Ground noise image examples. In this example 1 pixel is equal to 5 cm, so the 20-pixel noise image has 1-meter noise grain on the ground. Final composite image is shown at bottom right.

3.4.3.2 Synthetic Pulse Generation with Ground Noise

Once the ground noise properties were established, noise images were added to noise free synthetic pulse targets images with 6 degrees of angle from the north of image. Because SDSU has been using a 6-degree angle from true north since 2000 when the pulse and edge targets are laid out, this value was used again in these simulations. Eleven pulse edge contrast levels were developed as listed in Table 3.2 to obtain a variety of SNR values for the target. An example procedure plot is shown in Figure 3.10. The upper left image is the ground noise image with the sub-pixel noise pattern, and the upper right image is one of 11 levels of synthetic pulses with a 6-degree edge. Those two images were added and convolved with a known sensor model. The convolved image was resampled before processing with a pulse MTF estimator. For each edge transition level, a new noise image was generated and added to it.

Table 3.2. 11 Predetermined Pulse transition levels.

Pulse	1100	1000	950	900	850	825	800	790	780	775	770
Ground	400	500	550	600	650	675	700	710	720	725	730
Difference (Pulse – Ground)	700	500	400	300	200	150	100	80	60	50	40

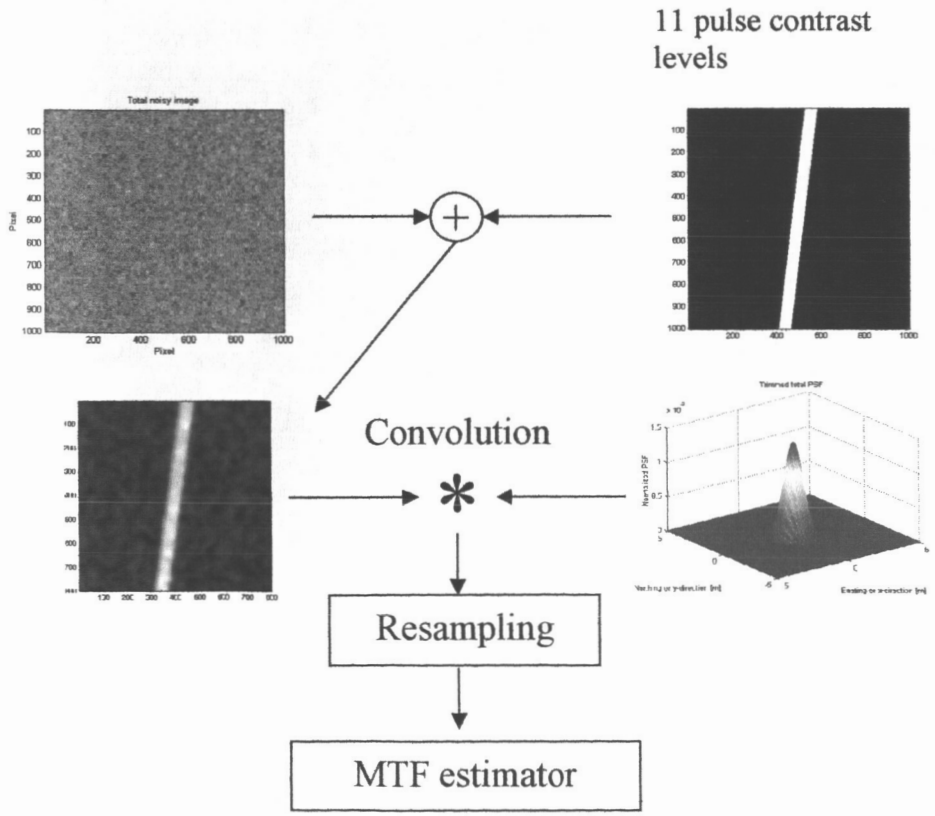

Figure 3.10. Noisy pulse target generation and MTF process.

3.4.3.3 Ground Noise Simulation Results

Ground noise simulation was performed in a system noise free situation. The ground noise simulation results are shown in Figure 3.11. The blue asterisks represent MTF values at Nyquist from twenty independent simulations at each of the eleven predetermined pulse contrast levels. The red line is the trueMTF value at Nyquist from the original PSF. The plot clearly shows the accuracy of the MTF estimate at Nyquist to improve with SNR. The data suggest that SNR > 50 is clearly desirable. SNR > 100 is preferred, with little improvement seen above that level. Once again, there is clearly a bias in the MTF estimate with MTF at Nyquist being underestimated at high SNR by almost 6 percent.

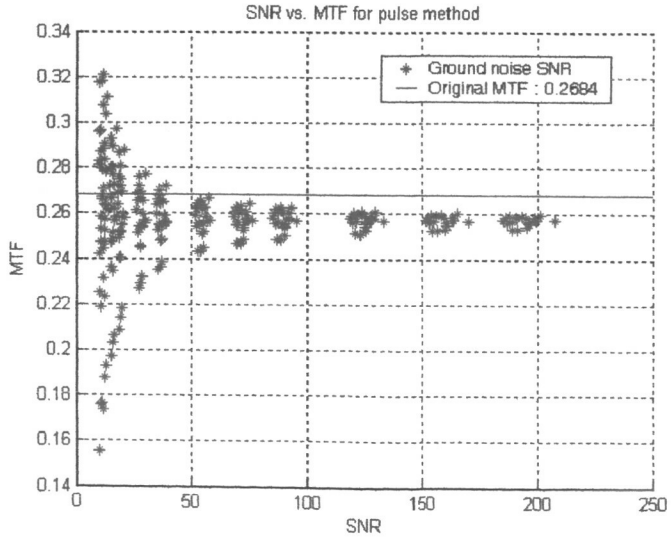

Figure 3.11. SNR vs. MTF value at Nyquist result plot from Ground noise edge target simulation.

3.5 Pulse Angle Simulation

In the previous noise simulations, a static MTF estimation error was observed. An assumption was made that this static error was caused by the target orientation from true North. To determine the relationship between static error of MTF values at Nyquist frequency and target angle, a set of 120 synthetic pulses were developed with target angles from 2 to 14 degrees with a step of 0.10 degrees. Those synthetic images were processed by the sensor model and re-sampled to a 1 meter GSD. Finally, the MTF values at Nyquist were plotted as a blue solid line in Figure 3.12 as a function of the target angle calculated from the MTF estimator.

An MTF under-estimation was observed on a continually decreasing quadratic curve. This result indicated that target angle was a contribution factor to a static MTF estimation error. The curve trend from Figure 3.23 was insufficient to reach the original MTF value at zero target angle. This observation demonstrates that the bias is not caused by failing to take into account the increase in effective pulse width due to the orientation angle. Application of a cosine correction explains only a small portion of the error as shown from the curve in Figure 3.12.

Thus this angle simulation suggests that target angle is a factor in the static under-estimation of the MTF value at Nyquist. Further investigation is warranted to determine if a synthetic correction is possible.

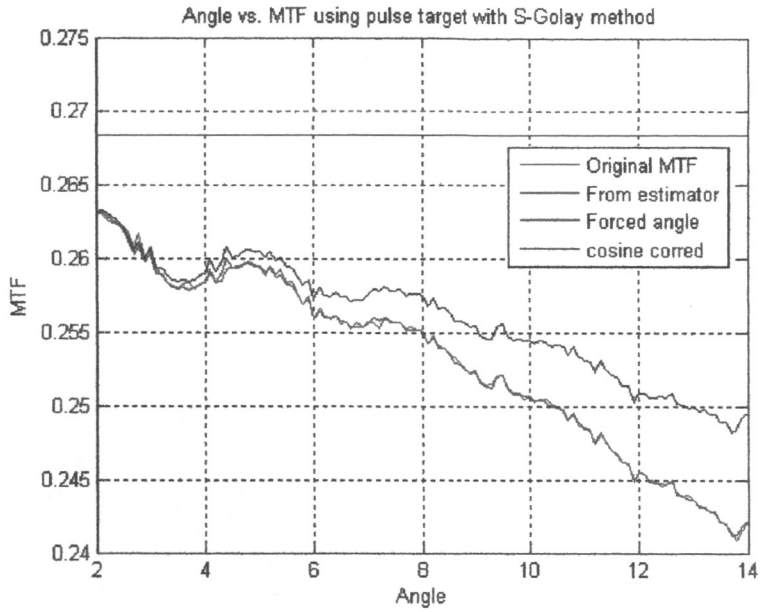

Figure 3.12. Pulse angle difference between true (forced) angle and estimated angle. The original MTF value is 0.2684.

3.6 Pulse Width Simulation

Although the processing steps of the edge and pulse methods are very similar, the pulse method requires an extra parameter called pulse width when it calculates the ratio between input and output. It turns out that the MTF estimate is very sensitive to this parameter, especially at certain frequencies. In this section, the MTF estimate sensitivity with input pulse width was studied with particular emphasis at the Nyquist frequency. Two possible scenarios were categorized based upon human errors. The first case considered that there could be a target measurment error but the true pulse target width was 3 pixels wide. Secondly, there could be physical layout error. In this case, the measurement of the pulse width was constantly 3 pixel wide, but the true pulse width was not three pixels. Both of those cases were simulated separately in the following sections.

3.6.1 Human Measure Error

The desired pulse width is exactly three-pixels wide. But when the target is measured, human errors creep in. To test pulse target width error sensitivity on MTF estimation

at the Nyquist frequency, human measurement error was considered to range from a pulse width of 2.75 pixels to 3.25 pixels with a step of 0.05 pixels. The measured pulse width determines the zero-crossing locations in the denominator of the ratio used in the MTF calculation. When the measured pulse width is smaller than actual pulse size, zero-crossing points shifted to higher frequencies as shown with the red solid line in Figure 3.13 below. The Nyquist frequency point at 0.5 normalized frequency is very close to the maximum of the first sidelobe. When the input pulse width is incorrectly measured as 3.25 pixels, the zero crossing shift to lower frequencies as shown by the black curve in Figure 3.13. In this case, the Nuquist frequency is shifted down on the high frequency side of the first sidelobe.

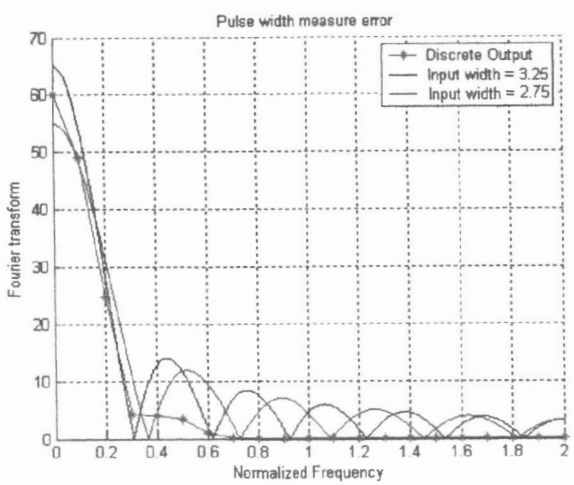

Figure 3.13. Sinc function change introduced by human measurement error when actual input width was 3 meters.

In the pulse method, MTF at Nyquist was calculated by taking the normalized ratio between the blue asterisks and the input sinc function value at 0.5 cycles per pixel with either the black or red line in Figure 3.13. Because the Nyquist point started on the left side of the first sidelobe peak and moves to the right as shown in Figure 3.14, the final MTF value at Nyquist is inversely related to the shape of slidelobe. The MTF response was exactly the same as the inverse of the red line in Figure 3.14 as shown in Figure 3.15. Fortunately, the magnitude of the error in MTF at Nyquist is small.

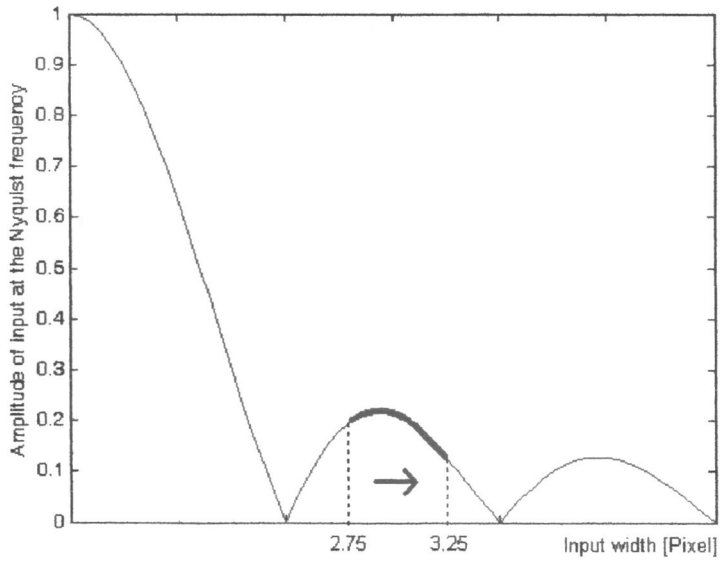

Figure 3.14. Nyquist location on input sinc function with human measure error from 2.75 to 3.25 pixels.

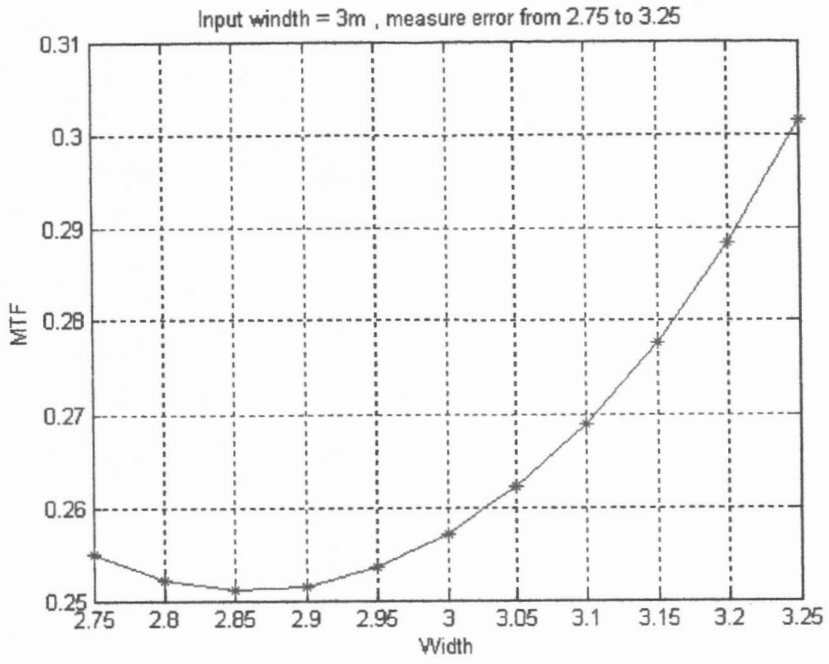

Figure 3.15. Value at Nyquist on input sinc function with human measure error from 2.75 to 3.25 pixels.

3.6.2 Systematic Width Error

The second simulation condition was that the actual width of the pulse was three pixels, but the input width in the processing system was changed by possible noise at the sensor, viewing angle, or various processing or resampling techniques, etc. In this case, the input sinc function was fixed in the plot but the sampled output plot was changed. The simulation range for the output pulse width was from 2.75 to 3.25 meters. Figure 3.16 shows a very similar response compared to the human error plot in Figure 3.14,

but the output sampled sinc function moved closer to the origin by increasing the pulse width from the sensor (or output width). Even though the sinc function shape and zero-crossing points are not clearly seen in the black and red output curves, the resulting plot shape in Figure 3.17 is the inverse of the curve shown in Figure 3.15 because the 'error in the output pulse width' case was opposite to the 'human error' case. As a result, Figure 3.17 shows an inverse shape compared to the previous case, as expected. Again, the magnitude of the error at Nyquist is small.

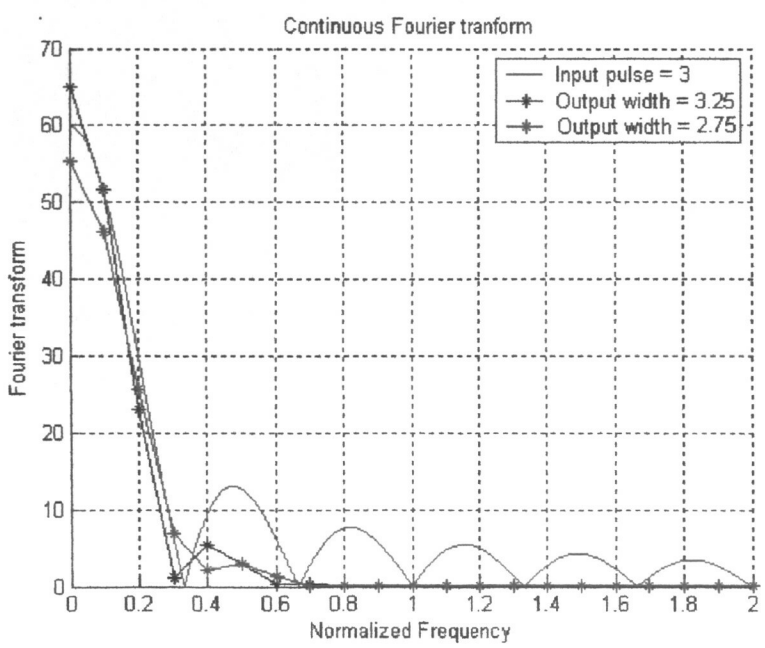

Figure 3.16. Result plot of error in output pulse width.

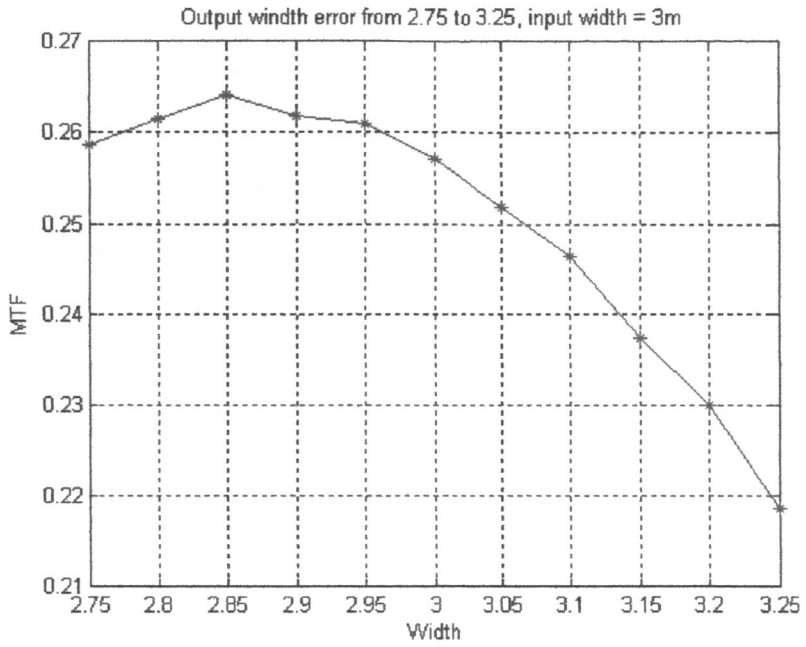

Figure 3.17. Value at Nyquist plot with output pulse error from 2.75 to 3.25 pixels.

3.6.3 Error Detection Scheme

Greater errors occur in the MTF estimate at 0.3 and 0.4 cycle/pixel due to pulse width measurement error because these frequencies are located much closer to the zero crossing of the sinc curve. Because the first zero-crossing occurs between these two frequencies, any small change of the Fourier transform of the output pulse is amplified in the final MTF plot. This simulation result

suggests that the noisy spikes occurring at these frequencies could be used to indicate potential measurement error in the pulse method process.

From observations of the preceding simulations, whenever the input pulse width was smaller than the measured value, the MTF value at 0.3 cycles / pixel was higher than the normal trend of a smooth MTF curve; and the MTF value at 0.4 cycles / pixel was lower than the normal MTF shape as shown in Figure 3.18. In the figure, the blue curve represents when input and output target widths were matching, and the red curve was generated when the measured input width was 2.8 meters and the output pulse width was 3.0 meters.

As an opposite case, Figure 3.19 shows the opposite result when the input pulse width is larger than the measured value. The MTF value at 0.3 cycles / pixel was lower than the normally trending curve, and the MTF value was higher at 0.4 cycles / pixel.

By testing abnormal trends at 0.3 and 0.4 frequency values, errors in pulse target width could be estimated and corrected. Note in each case (Figures 3.18 and 3.19) that the error in MTF at Nyquist is small.

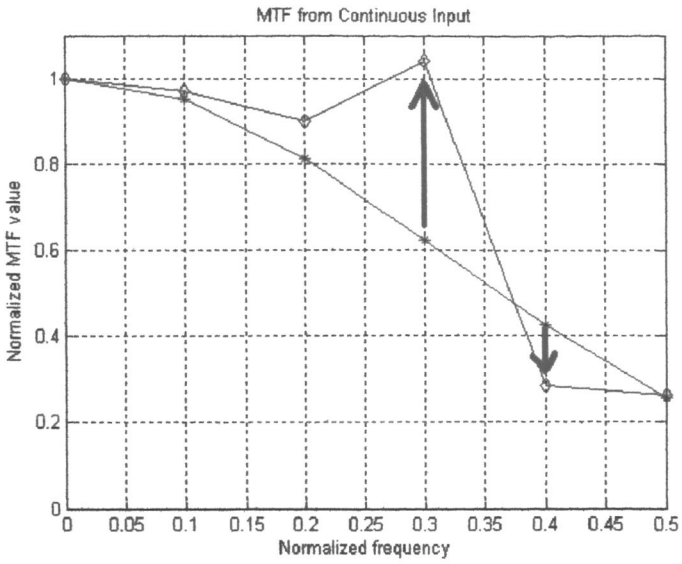

Figure 3.18. MTF plot deformation with larger input pulse width.

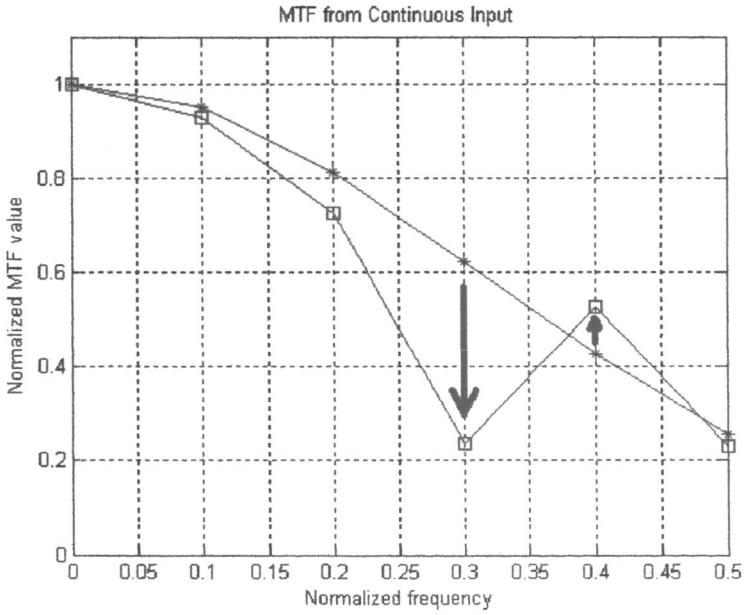

Figure 3.19. MTF plot degradation with smaller input pulse width.

3.6.4 Error Correction on 2002 Quickbird MTF Result

MTF plot shape deformations were reported previously in 2002 and 2003. Pulse width error detection and correction was only applicable to the images acquired in year 2002 because of the GSD change in 2003 from 2.8 to 2.4 meters without notice. The GSD change made the sampling grid finer which produced a larger pulse width in the output images. The sinc function from Fourier transformation of the larger pulse placed the Nyquist frequency location very close to the second zero-crossing point. Because the behavior of the error detection process was hard to predict in this sutuatuion, pulse width error corrections were applied only to 2002 Quickbird images.

An example of MTF from previous work is shown in Figure 3.20. By testing the response at 0.3 and 0.4 cycles / sample, it was concluded that an under-estimation of the tarp width occurred during previous analyses. In other words, the MTF plot in Figure 3.20 had a shape similar to the red curve in Figure 3.19 which suggested the ground measurement was smaller than the actual tarp width. Several tarp width values were tested and it was determined that a new tarp width of 8.95 meters gave smoother transitions than the old tarp width of 8.83 meters. Figure 3.21 shows Fourier transformation of input and output

signals with the original tarp width of 8.83 meters in red and the modified tarp width of 8.95 meters in green. Although the change in the frequency domain seemed minor,

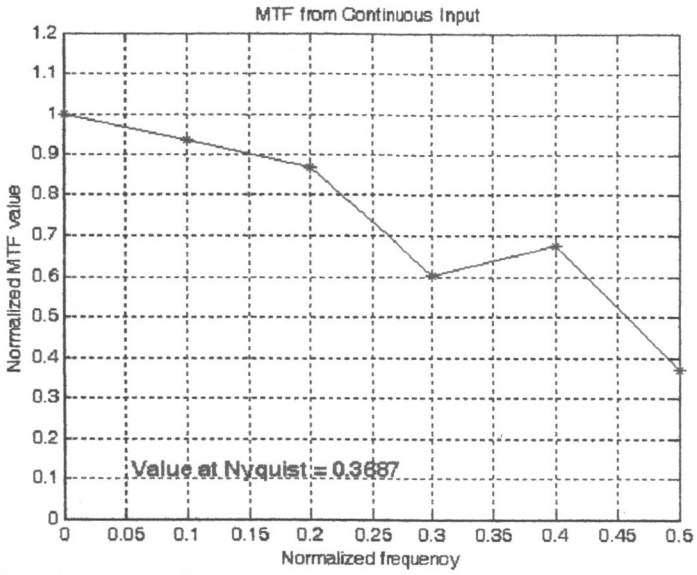

Figure 3.20. An MTF plot from SDSU pulse target on September 15, 2002 imaged by Quickbird satellite.

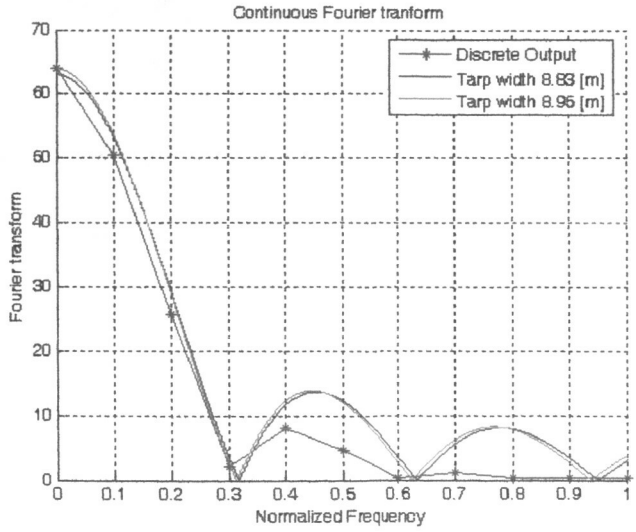

Figure 3.21. Sinc function comparison between old and new tarp width with the QuickBird image on September 15, 2002.

this small change corrected the MTF plot dramatically as shown in Figure 3.22. The value at Nyquist changed from 0.3678 to 0.3809 which was 3.6%.

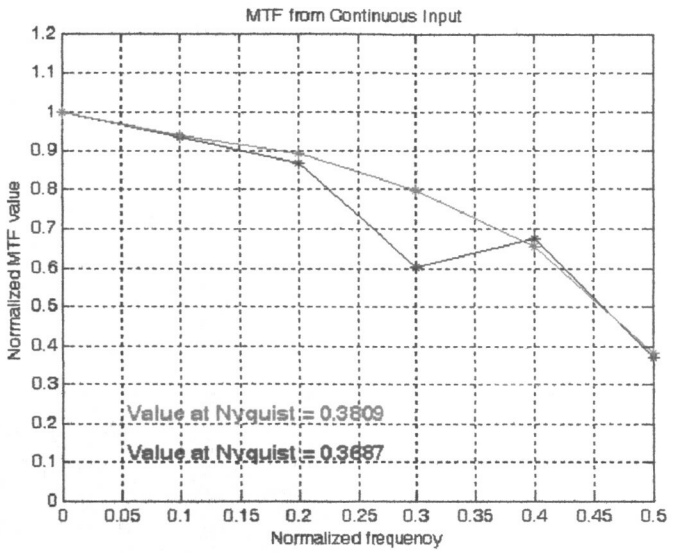

Figure 3.22. MTF overplot between old and new tarp width with the QuickBird image on September 15, 2002.

Pulse width error detection and correction was applied to other Quickbird images on July 20 and September 7, 2002 and the results are shown in Figure 3.23. The MTF profiles before correction indicated that tarp widths were underestimated as shown in Table 3.3. These corrections were applied on three 2002 Quickbird scenes, with the result that the value at Nyquist was very stable--within 4% after width correction. The stability at the Nyquist frequency was considered during the original design of the pulse method. The reason for Nyquist frequency stability

is apparent in the sinc function overplots shown in Figure 3.24. Note the very small change at 0.5 cycles / pixel when the pulse width changes from 2.75 to 3.25 pixels. Large changes occurred at 0.3 and 0.4 cycles / pixel as indicated by red and blue arrows, which resulted in the large MTF shape deformation.

Table 3.3. Pulse width error detection and correction applied on July 20 and September 7, 2002 Quickbird MTF plots

Date	Original Width	Corrected Width	Percent difference
July 20, 2002	0.3333	0.3399	1.98%
September 7, 2002	0.3687	0.3809	3.30%

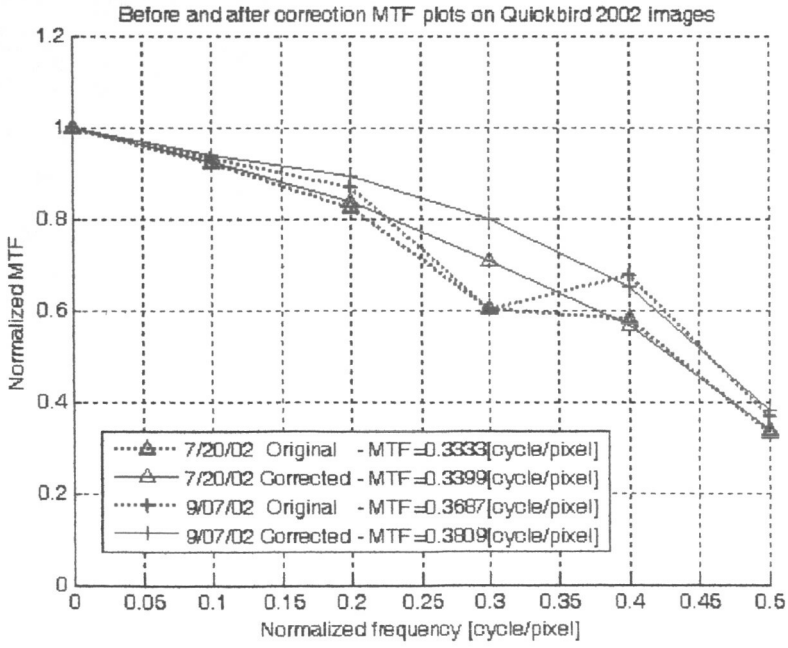

Figure 3.23. Pulse width error detection and correction applied on July 20 and Sept. 7, 2002 Quickbird images.

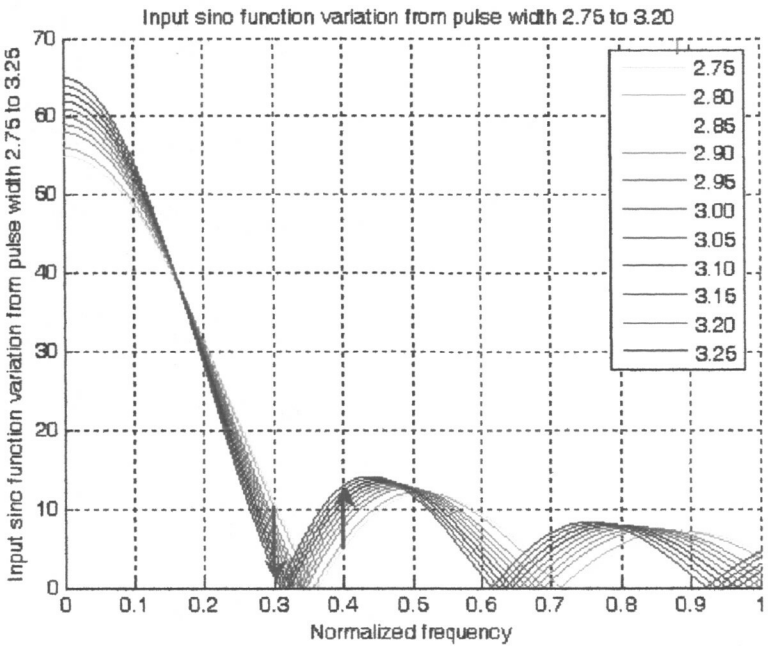

Figure 3.24. Sinc function change according the input pulse width error to the estimator. The original tarp width was fixed at 3 pixel wide.

4 Conclusions

As a part of continuing research in generic sensor modeling, the pulse MTF estimator was tested and characterized using Fermi edge detection and 4^{th} order MSG filtering.

Based on the known PSF, the performance of pulse MTF estimator provided 4.1% under-estimation compared to the original PSF in a noise free situation.

System and ground noise sensitivity simulation produced relationships between SNR and the MTF value at Nyquist. Two different approaches converged to agreement that a minimum SNR of 50 was required to get reliable MTF estimation using the pulse method.

From the pulse angle sensitivity simulation, one source of the static error between original and estimated MTF values at Nyquist was caused by the 6-degree angle of the edge target. This bias was reduced when the edge angle was close to zero. But this compromises target length and the number of edge transition pixels.

By the very nature of the sinc function in the pulse method, the MTF values at 0.3 and 0.4 cycles / pixel are easily skewed by any width measurement error. This

disadvantage of using the pulse target also provided a way of measuring this error and correcting it.

The generic sensor model provided an excellent simulation environment to obtain artificial responses for various situations that occur in actual field campaign. Due to use of this modeling tool, a number of significant estimator error sources are now well understood and, in many cases, corrections have been developed. This sensor model could be used for further study such as for aliasing errors, other MTF estimator methods, and so on.

References:

[1] Coltman, J. W., 1954. The Specification of Imaging Properties by Response to a Sine Wave Input. J. Opt. Soc. Am. 44, pp. 468-471.

[2] Kaftandjian, V., 1996. A Comparisons of the Ball, Wire, Edge, and Bar/Space Pattern Techniques for Modulation Transfer Function Measurements of Linear X-Ray Detectors. Journal of X-ray Science and Technology. 6, pp. 205-221.

[3] Schowengerdt, R. 1985. Operational MTF for Landsat Thematic Mapper. SPIE Image Quality: An Overview, 549, pp. 110-116

[4] Dennis L. Helder, "In-flight Characterization of Spatial Quality Using Point Spread Functions," ISPRS proceedings of the international workshop on radiometric and geometric calibration, 2-5 Dec 2003, pp. 151-170

[5] Rafael Gonzalez, "Digital Image Processing" Addison-Wesley, 1993, Page 208~209.

[6] Alexis P. Tzannes, Jonathan M. Mooney, "Measurement of the modulation transfer function of infrared cameras," Optical Engineering, Vol. 34 No. 6, June 1995, Page 110~116.

[7] William Press, "Numerical Recipes in C," Cambridge University Press, 2002, 2nd edition, Page 650~655.

[8] *Optimisation Toolbox For Use with MATLAB - User's Guide.* Nattick, MA: The Mathworks, Inc., web site: www.mathworks.com, Online PDF version, pp. 4-54 - 4-57, June 2001.